Spontaneous Nernst effect in the iron-based superconductor $Fe_{1+y}Te_{1-x}Se_x$

Lu Chen,[1,*] Ziji Xiang,[1] Colin Tinsman,[1] Bin Lei,[2] Xianhui Chen,[2] G. D. Gu,[3] and Lu Li[1,†]

[1]*Department of Physics, University of Michigan, Ann Arbor, 450 Church Street, Ann Arbor, Michigan 48108, USA*

[2]*Hefei National Laboratory for Physical Science at Microscale and Department of Physics, University of Science and Technology of China, Hefei 230026, China*

[3]*Brookhaven National Laboratories, Upton, New York 11973, USA*

(Received 10 October 2019; revised 24 July 2020; accepted 23 July 2020; published 6 August 2020)

We present a study of the Nernst effect in an iron-based superconductor with a nontrivial band topology $Fe_{1+y}Te_{1-x}Se_x$. A nonzero Nernst signal is observed in a narrow temperature region around the superconducting transition temperature T_c at a zero field. This anomalous Nernst signal shows symmetric dependence on the external magnetic field and indicates an unconventional vortex contribution in an *s*-wave superconductor with a strong spin-orbit coupling, which is originated from the local magnetic moments of the interstitial Fe atoms. Our experiments also provide the first evidence of a locally broken time-reversal symmetry in bulk $Fe_{1+y}Te_{1-x}Se_x$ single crystals.

DOI: 10.1103/PhysRevB.102.054503

Topological superconductors have attracted tremendous attention due to their potential of hosting Majorana zero modes (MZM) and further application in topological quantum computation [1,2]. The theory has predicted that the iron-based superconductor $Fe_{1+y}Te_{1-x}Se_x$ could host a topological superconducting state on its surface [3–5], which was demonstrated in photoemission [6] and scanning tunneling spectroscopy measurements [7]. Apart from the Dirac dispersion in the surface state, a zero-energy bound state (ZBS) has also been observed at magnetic-field-induced vortices in $Fe_{1+y}Te_{1-x}Se_x$ [7–9], which indicates a Majorana bound state. Even more surprisingly, the robust ZBS was also found at each interstitial iron impurity by scanning tunneling microscopy in the absence of an external magnetic field [10]. Recently, Jiang *et al.* proposed a theoretical explanation that magnetic impurity ions can generate topological vortices without external magnetic fields in *s*-wave superconductors with strong spin-orbit coupling. These quantum anomalous vortices (QAVs) can even support robust Majorana zero modes when the topological surface states are superconducting [11]. We are curious about how the topological vortices could affect the vortex flow in the vortex liquid state of a type-II superconductor. The best way is to conduct the Nernst effect measurement.

In this paper, we report on a study of Nernst effect in an iron-based superconductor $Fe_{1+y}Te_{1-x}Se_x$. We observe a zero-field Nernst effect that appears around the superconducting transition temperature T_c. This spontaneous Nernst signal does not follow the temperature and field dependence of the thermal power, and occurs only in the T range near T_c where the superconducting fluctuation is strong and vortex liquid is robust. This intrinsic spontaneous Nernst signal indicates the violation of local time-reversal symmetry (TRS) in the superconducting state. The TRS in $Fe_{1+y}Te_{1-x}Se_x$ may be broken by pinning flux introduced by the interstitial iron impurity. To further understand the role of excess Fe atoms, we study a series of $Fe_{1+y}Te_{1-x}Se_x$ single crystals that have different T_c and different levels of excess Fe concentrations and demonstrate how they affect the spontaneous Nernst effect signal.

The single crystals of the $Fe_{1+y}Te_{1-x}Se_x$ were grown by using a unidirectional solidification method [12]. There are different superconductivities for different sectional crystals in the grown ingot in which the actual composition and extra iron in the crystals are variable. The as-grown $Fe_{1+y}Te_{1-x}Se_x$ single crystals were sealed in a vacuum quartz tube and annealed at 400 °C $\sim$ 450 °C for 6 days to 50 days to make the Se/Te distribution more homogeneous (see the Appendix for more details). Three sets of crystals are studied. The first set (sample 1) generally has the highest T_c and lowest bulk resistivity. The second set (samples 2, 3, 4, and 5) has lower T_c and larger bulk resistivity. The third set is superconducting without annealing. Named as sample 6, they are usually without shinning surfaces and are argued to be crystals without excess Fe [7]. The elemental composition of the samples is analyzed with the energy-dispersive x-ray spectroscopy (EDX). (We note, however, transport measurements and EDX measurements cannot exclude the existence of a small level of excess Fe in these nominally Fe-impurity-free samples.) The dimensions for all six samples are listed in Table I of the Appendix. The Nernst and Seebeck effects were measured using the pulsed-power technique [13,14] in a Physical Properties Measurement System (PPMS) DynaCool from Quantum Design and the Oxford Triton200-10 Cryofree Dilution Refrigerator. The signals are checked with static state method, in which the heating current is varied and the thermoelectric voltage signals are proportional to the heating power. In our geometry, the temperature gradient $-\nabla T$ is applied in the *ab* plane of the crystal ($-\nabla T \parallel \hat{\mathbf{x}}$). With a magnetic field along

*chelu@umich.edu
†luli@umich.edu

TABLE I. Properties of $Fe_{1+y}Te_{1-x}Se_x$ samples 1 to 6.

Sample	Formula	T_c	SFV	Sample dimension $(L \times W \times t)$ mm^3
1	$Fe_{1+y}Te_{0.65}Se_{0.34}$	14.39 K	88.8%	$4.4 \times 1 \times 0.15$
2	$Fe_{1+y}Te_{0.6}Se_{0.4}$	14.24 K	82.5%	$3.5 \times 1.2 \times 0.075$
3	$Fe_{1+y}Te_{0.61}Se_{0.39}$	13.15 K	73.2%	$3 \times 1.2 \times 0.125$
4	$Fe_{1+y}Te_{0.58}Se_{0.41}$	13.39 K	74%	$3.5 \times 2 \times 0.0875$
5	$Fe_{1+y}Te_{0.56}Se_{0.42}$	13.75 K	1.7%	$5 \times 1.5 \times 0.1$
6	$FeTe_{0.6}Se_{0.4}$	14.02 K	92.6%	$3 \times 1.5 \times 0.4$

the crystal c axis ($H \parallel \hat{\mathbf{z}}$), the voltage measured along $\hat{\mathbf{y}}$ gives the raw Nernst signal e_N [15–19], $e_N = \frac{V_y(B,T)}{|-\nabla T|d}$, in which d is the distance between the two voltage leads. Since there is always inevitable pickup of Seebeck signals in the Nernst effect measurement due to the misalignment of contact leads, we have to subtract the Seebeck signal from the raw Nernst signal to reveal the intrinsic Nernst signal.

Following the pioneering work [20], we determine the geometric pickup factor by scaling the S-T curves to match the e_N-T curves in the normal state [as shown in Fig. 1(a)]. This step assumes that there is no intrinsic zero-field Nernst effect signal in the normal metallic state, and the resulting

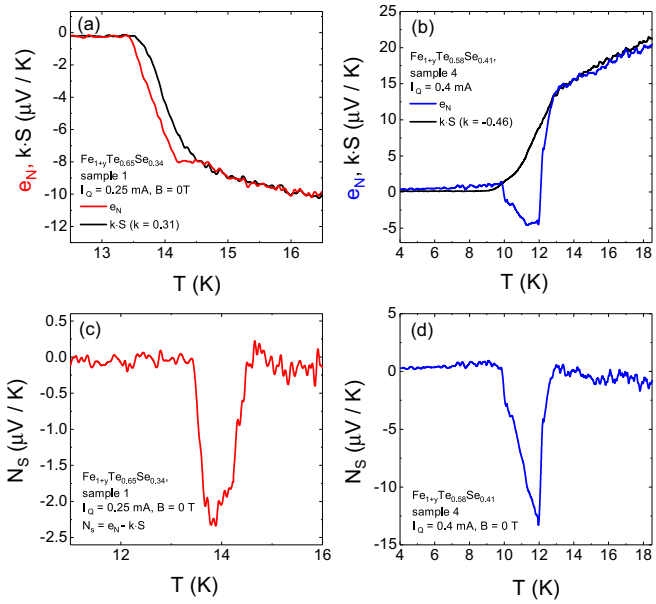

FIG. 1. The zero-field thermoelectric responses of topological superconductor $Fe_{1+y}Te_{1-x}Se_x$. (a) Temperature T dependence of the thermopower kS (Seebeck signal) and the observed Nernst signal e_N in sample 1. The thermopower signal S was scaled by a factor $k = 0.31$ to match the T dependence of S and e_N. (b) The same T dependence of S and e_N for sample 4, which is in different batch and with different T_c. Similar to sample 1, sample 4 also shows that the observed Nernst signal e_N matches the thermopower signal S very well at $T > T_c$. However, a sharp peak appears around T_c. For both samples, the intrinsic spontaneous Nernst signal is extracted by subtracting the scaled thermopower signal $N_S(T) = e_N(T) - kS(T)$. (c), (d) Plot the intrinsic spontaneous Nernst signals N_S vs T in samples 1 and 4. The heater resistance is 1 kΩ for both samples.

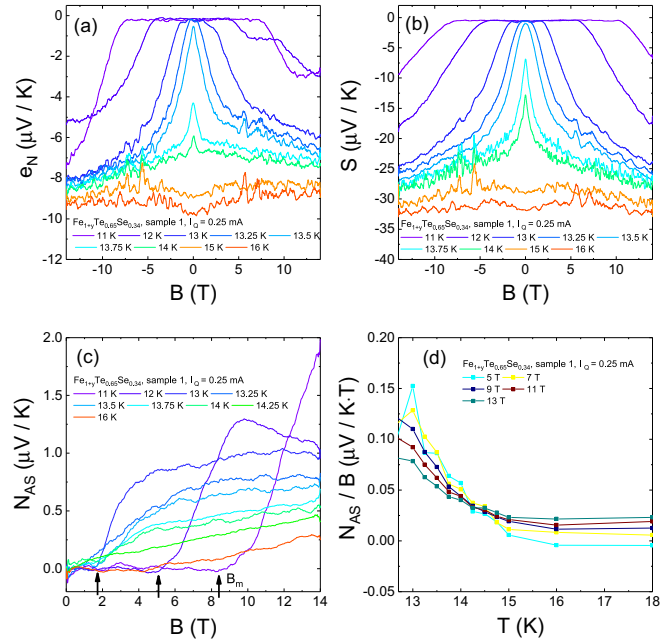

FIG. 2. Observed (a) Nernst signal e_N and (b) Seebeck signal vs magnetic field B at selected T from 11 to 16 K in sample 1. (c) Ordinary Nernst signal N_{AS} of sample 1 following the standard B antisymmetrization to curves in (a). Arrows indicate the melting field B_m of the vortex solid state. (d) Temperature dependence of the ordinary Nernst coefficient $\frac{N_{AS}}{B}$ at selected B up to 13 T. The heater resistance is 1 kΩ.

scaling factor k reflects simply the (small) geometric factor due to the transverse contract misalignment. The intrinsic Nernst signal N_S is given by subtracting the thermopower signal, viz.,

$$N_S(B,T) = e_N(B,T) - kS(B,T) \quad (1)$$

in which k is a geometrical scaling factor. The geometrical scaling factor should be the same when the temperature is above or below the superconducting transition temperature since phonon dominates the heat transfer at such a temperature range (more details can be found in the Appendix). After subtracting the Seebeck signal, the intrinsic Nernst signal shows a prominent peak between 13.5 and 14.5 K [Fig. 1(c)]. This zero-field Nernst signal can be repeated in other $Fe_{1+y}Te_{1-x}Se_x$ samples with different Fe concentration. For example, N_S in sample 4 is larger than the signal in sample 1, as shown in Fig. 1(d). We will discuss the effect of Fe concentration on the magnitude of spontaneous Nernst signal later in this paper. The spontaneous Nernst signal also shows some fluctuation even within the same sample. The sign and magnitude of the spontaneous Nernst signal vary at different channels in the same sample (as shown in Fig. 8 in the Appendix).

To study the field dependence of the Nernst effect, we measured the Seebeck and Nernst signal simultaneously in a magnetic field up to 14 T. Figure 2(a) shows the raw Nernst signal e_N vs B in sample 1 at several selected temperatures across the superconducting transition. e_N shows an antisymmetric behavior with respect to B. The ordinary Nernst signal is obtained by the field antisymmetrization to the Nernst curves

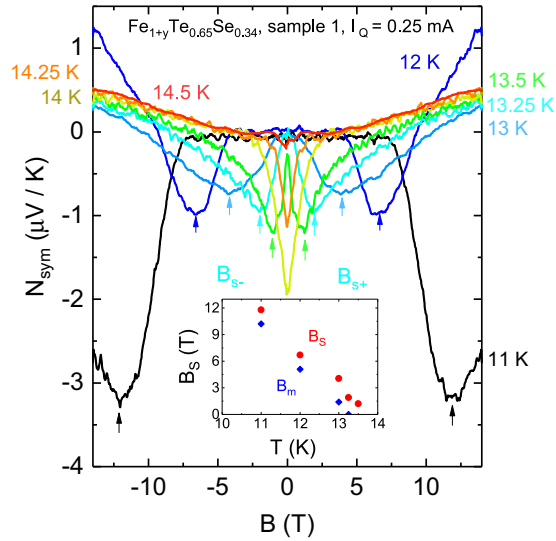

FIG. 3. Magnetic field dependence of the intrinsic field-symmetrized Nernst signal. The Seebeck pickup has been subtracted [see Eq. (1)]. Arrows indicate the location of the shoulder trend B_S. Inset shows the temperature dependence of B_S, compared with the melting fields B_m. As expected for the characteristic field scales in superconductors, both fields converge to zero as the T increases toward T_c. The heater resistance is 1 kΩ.

in Fig. 2(a), i.e., $N_{AS} = \frac{1}{2}[e_N(B,T) - e_N(-B,T)]$ [shown in Fig. 2(c)]. Above T_c, the ordinary Nernst signal becomes larger with decreasing T. At $T < T_c$, the ordinary Nernst signal starts at zero at low fields. Once B increases beyond the characteristic field B_m, the ordinary Nernst signal increases to finite, reflecting the magnetic-field-driven transition from the vortex solid state at the low fields to the vortex liquid state in the high fields. The sign of the high-field ordinary Nernst effect signal is consistent with that of the moving vortices [15,17]. Finally, we plot the T dependence of ordinary Nernst coefficient N_{AS}/B at selected fields in Fig. 2(d): the results are consistent with the previous study [21]. The ordinary Nernst coefficient is strongly enhanced inside the vortex liquid state and vanishes gradually once it enters the vortex solid state. Its peak shifts to lower temperature at a higher field, which is similar to the behavior of thermally driven vortices in cuprate [18,22,23], organic [24], and conventional superconductors [25].

Aside from the ordinary Nernst signal, Fig. 2(a) also contains information about the field dependence of the anomalous Nernst signal shown in Fig. 1(c). By subtracting the Seebeck pickup kS and ordinary Nernst signal N_{AS} from the observed Nernst data e_N, we obtain the anomalous Nernst signal $N_{\rm sym}$, viz.,

$$N_{\rm sym}(B,T) = e_N(B,T) - kS(B,T) - N_{AS}(B,T). \quad (2)$$

This process is equivalent to subtract the Seebeck pickup from the raw Nernst signal and then do a field symmetrization. The anomalous Nernst signal $N_{\rm sym}$ is plotted in Fig. 3, which shows a symmetric pattern with respect to B. $N_{\rm sym}$ is nonzero as $B \to 0$, which decreases as T increases from 11 to 14 K. This trend of $N_{\rm sym}$ at zero field is consistent with the T dependence of the spontaneous Nernst signal plotted in Fig. 1(c). Another important feature about the anomalous Nernst signal $N_{\rm sym}$ is a deep trench centered at $B = 0$ T. The trench becomes narrower as T increases from 11 K. This field-symmetric Nernst signal also shows broad dips that shift to lower field as T increases. We indicate the location of theses broad dips by B_S and plot the temperature dependence of B_S in the inset of Fig. 3. B_S gradually converges to zero field as T increases. This trend is similar to the T dependence of the melting field B_m, suggesting the vortex nature of the anomalous Nernst signal.

Theoretically speaking, such a zero-field Nernst signal is forbidden in a material that holds the TRS. A broken time-reversal symmetry (TRS) has been theoretically predicted in many high-T_c superconductors, such as cuprates [26,27] and iron-based superconductors [28–31]. In cuprates, the broken TRS is observed by angle-resolved photoelectron spectroscopy (ARPES) [32], polarized neutron scattering [33–35], Nernst measurements [20,36], and magneto-optical measurements [37–39]. As for the iron-based superconductors, there is less evidence about the spontaneous breaking of TRS. Grinenko *et al.* reported the observation of an enhanced zero-field muon spin-relaxation rate below the superconducting transition temperature in the ion-irradiated $Ba_{0.27}K_{0.73}Fe_2As_2$ single crystals [40]. There is no experimental evidence of TRS breaking in the bulk of intrinsic Fe-based superconductors. In $Fe_{1+y}Te_{1-x}Se_x$, the excess Fe randomly occupies the Fe(2) site between the square planar sheets of Fe [41,42]. The interstitial iron impurity could locally break the TRS by introducing a local magnetic moment [43]. Although the Nernst effect is generally taken as a bulk transport measurement probe, it often reflects the fluctuations in the local scale (a good example is the superconducting fluctuation in the cuprates [15,44–47]). The Nernst signal only measures the local thermoelectric properties across each channel, which is consistent with the variation of the spontaneous Nernst signal observed among different Nernst channels in the same $Fe_{1+y}Te_{1-x}Se_x$ sample (see Fig. 8 in the Appendix). We believe the difference in different Nernst channels is exactly caused by the uneven distribution of iron impurities across the sample. The iron impurity is not evenly distributed across the whole sample, which is observed in our EDX measurement. The most reasonable interpretation of why we see almost absent spontaneous Nernst signals on some channels in part of our $Fe_{1+y}Te_{1-x}Se_x$ samples is that the spin-up and spin-down moments on excess iron sites are almost compensated locally at the positions of these channels.

To understand how the amount of excess Fe could affect the zero-field Nernst signal, we measured the Nernst effect in a series of $Fe_{1+y}Te_{1-x}Se_x$ samples with different Fe concentration. In these $Fe_{1+y}Te_{1-x}Se_x$ single crystals, the atomic concentration is determined by the EDX measurement with a Cameca SX100 Electron Probe Micro Analyzer. For each sample, we select 15 spots on the sample to do EDX measurement and get the averaged element concentration. The averaged Fe concentrations in four different samples (samples 2, 3, 4, and 5) are plotted in Fig. 4(a). The averaged peak values of the zero-field spontaneous Peltier Hall signal $|\theta^P|$ is defined as the ratio of $|\alpha_{xy}|$ and α_{xx} [48], in which α is the two-dimensional Peltier conductivity tensor. The Hall signal is very small compared to the resistivity within the

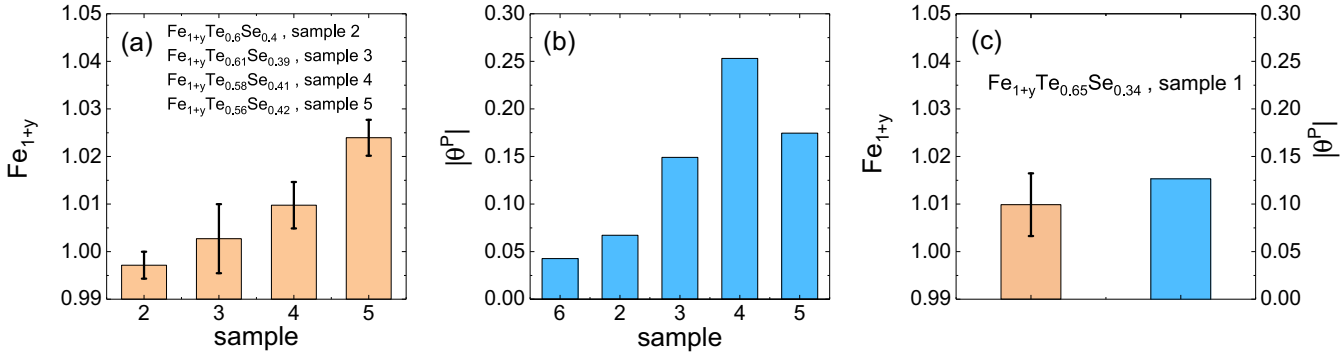

FIG. 4. (a) Fe concentration in $Fe_{1+y}Te_{1-x}Se_x$ samples 2, 3, 4, and 5. Error bars plot the standard deviation of Fe concentration on different sample spots. (b) The averaged peak values of the zero-field spontaneous Peltier Hall signal $|\theta^P|$, defined as the ratio of $|\alpha_{xy}|$ and α_{xx}, in samples 6, 2, 3, 4, and 5, in the order that the nominal Fe concentration increases. As a comparison, iron concentration and $|\theta^P|$ in sample 1 are also plotted in (c). Samples 2, 3, 4, and 5 have a lower Te concentration compared to sample 1.

temperature range where it shows spontaneous Nernst signal (as shown in the Appendix, $\rho_{xy}/\rho_{xx} < 0.01$). So the Hall angle θ can be negligible here [see Eqs. (A2) and (A3)]. The Peltier Hall signal $|\theta^P|$ in sample 2 to sample 6 is plotted in Fig. 4(b), which shows a nonmonotonic dependence on the Fe concentration. Sample 6 has nominally no excess Fe and the smallest $|\theta^P|$. As the Fe concentration increases, $|\theta^P|$ is first enhanced and then suppressed. The Fe concentration and $|\theta^P|$ measured in sample 1 are plotted in Fig. 4(c) as a comparison.

This spontaneous Nernst signal is only nonzero inside the vortex liquid regime. A similar anomalous Nernst effect has been reported in the striped cuprate superconductor $La_{2-x}Ba_xCuO_4$ (LBCO) by Li *et al.* [20]. In quasi-two-dimensional (quasi-2D) superconductors, thermally driven vortices are generated in equilibrium at $B = 0$ above the Berenzinski-Kosterlitz-Thouless (BKT) transition. Instead of having the same number of vortices and antivortices, a predominant sign of vortex is energetically favorable due to the relief of interlayer phase frustration [49]. In $La_{2-x}Ba_xCuO_4$, the strong superconducting fluctuation extends from the charge-ordering temperature down to 5 K enables the vortices (with the predominant sign) to move freely in a temperature gradient and generate the spontaneous Nernst signal [50,51]. The existence of the thermal-driven vortices has also been generally reported in Fe-based superconductors [21,52,53]. We note that $Fe_{1+y}Te_{1-x}Se_x$ is more toward a three-dimensional (3D) superconductor due to a weaker anisotropy [54]. Nonetheless, a theoretical study points out the existence of vortex liquid state in a three-dimensional type-II superconductor with strong thermal fluctuations [55]. As a result, for 3D anisotropic superconductors, such as $Fe_{1+y}Te_{1-x}Se_x$, there is still a narrow region between the superconducting critical temperature and the mean-field transition temperature where spontaneously created vortex lines exist [56]. This is consistent with the temperature span of a few Kelvin of the spontaneous Nernst signal observed in Figs. 1(c) and 1(d).

After having spontaneously generated vortex-antivortex pairs, the next question is what provides the nonzero net vortex in the vortex liquid state of $Fe_{1+y}Te_{1-x}Se_x$? Recently, Jiang *et al.* points out that in an *s*-wave superconductor with strong spin-orbit coupling, the magnetic impurity ions can generate topological vortices without applying a magnetic field [11]. The QAVs produced by the interstitial magnetic Fe are pinned at the magnetic ion, which means they can not move freely or provide the nonzero Nernst signal at zero field directly. The pinned quantum anomalous vortices could possibly break the balance between thermally created vortices and antivortices. Although we need further theoretical evidence to support this assumption, experimentally we find the spontaneous Nernst effect signals need both bulk superconductivity and excess Fe. This point is supported by the smallest signal amplitude of sample 6, the sample with the lowest excess Fe level [Fig. 4(b)]. This point is further supported by the observation that the spontaneous Nernst signal is strongly suppressed in sample 5 [as shown in Fig. 4(b)], which has a less than 2% superconducting volume (as seen in detail in Table I in the Appendix). This could be evidence that bulk superconductivity is indispensable in producing the spontaneous Nernst signal. As shown by a previous study, the as-grown $Fe_{1+y}Te_{1-x}Se_x$ single crystals hold filamentary superconductivity due to the extra Fe, most of the bulk nature of the superconductivity can only be achieved by oxygen annealing [57].

We also conduct the same thermoelectric measurements in FeSe single crystals which have similar properties as $Fe_{1+y}Te_{1-x}Se_x$ but a topologically trivial band structure [58]. The normal *B*-antisymmetric Nernst effect is consistent with early reports [59]. No obvious zero-field Nernst signal across the superconducting transition has been observed in FeSe single crystals. The field-dependent Nernst signal shows a monotonic dependence on the magnetic field, which contradicts to what has been observed in the $Fe_{1+y}Te_{1-x}Se_x$ samples. More details can be found in Fig. 14 in the Appendix. There is experimental evidence that shows the interstitial Fe(2) site is unoccupied in clean FeSe single crystals [60]. The absence of the spontaneous Nernst effect in FeSe is most likely due to the unoccupation of the interstitial Fe(2) site in FeSe single crystals. But, we could not rule out the possibility that a topologically nontrivial band structure also plays a role in inducing a spontaneous Nernst effect in $Fe_{1+y}Te_{1-x}Se_x$.

At this point, it is necessary to clarify that the zero-field spontaneous Nernst signal does not come from the disorder or inhomogeneity of the sample. Our $Fe_{1+y}Te_{1-x}Se_x$ and FeSe samples have similar superconducting transition width,

which means they have similar disorder levels. But, FeSe sample does not show the zero-field spontaneous Nernst signal, which indicates this signal does not simply come from the disorder or inhomogeneity of the sample. Furthermore, the inhomogeneity and nanoscale electronic disorder in the high-T_c superconductors has been observed in many cuprates [61–63]. But, it does not generally induce a spontaneous Nernst signal in the vortex liquid states of these cuprates, which indicates the spontaneous Nernst signal is an intrinsic property of $Fe_{1+y}Te_{1-x}Se_x$. The spontaneous Nernst signal does not come from the misalignment of the Nernst channel contacts or the pickup of anisotropic thermopower signal, either. The homogeneity of the temperature gradient in our sample is also checked with the thermal Hall measurements, and no thermal Hall signal has been observed within our resolution (as shown in Fig. 15 in the Appendix). More details about these discussions can be found in the Appendix.

To conclude, we study the Nernst effect in Fe-based superconductor $Fe_{1+y}Te_{1-x}Se_x$ and find a field-symmetric Nernst signal which is nonzero as $B \to 0$ and only appears in the superconducting state. Our experiment provides the first evidence of a locally broken TRS in the bulk of a topologically nontrivial superconductor. The spontaneous Nernst signal varies in different Nernst channels and the overall strength is sensitive to the concentration of excess Fe, suggesting its relevance to the TRS-breaking local moments on these interstitial Fe sites. Our results also indicate an unconventional vortex contribution and provide indirect evidence of the existence of QAVs, although more theoretical explanation is needed to illustrate the underlying mechanism.

ACKNOWLEDGMENTS

We thank X. Dai, L. Fu, and S. Kivelson for fruitful discussion. We also thank the Electron Microbeam Analysis Lab in the University of Michigan and its laboratory manager O. Neill for the support in the EDX measurements. This work at Michigan is mainly supported by the National Science Foundation under Award No. DMR-1707620 (transport measurement), by Department of Energy under Award No. DE-SC0020184 (magnetization measurements), by the Office of Naval Research through DURIP Award No. N00014-17-1-2357 (magnet and other instruments for the dilution refrigerator), and by the National Science Foundation Major Research Instrumentation under Award No. DMR-1428226 (the equipment of the transport characterizations). The work at Brookhaven is supported by the Office of Basic Energy Sciences, Materials Sciences, and Engineering Division, U.S. Department of Energy (DOE) under Contract No. DE-SC0012704. B. Lei and X. Chen thank the National Natural Science Foundation of China (Grant No. 11888101) and the National Key Research and Development Program of the Ministry of Science and Technology (Grant No. 2017YFA0303001) for support.

APPENDIX: MATERIALS AND METHODS

1. Sample preparation

The single crystals of the $Fe_{1+y}Te_{1-x}Se_x$ were grown by a unidirectional solidification method. There are different

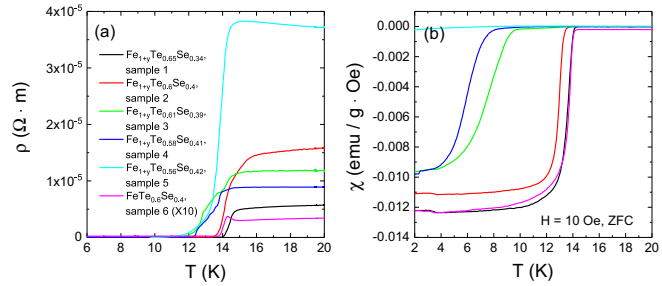

FIG. 5. (a) Resistivity and (b) zero-field-cooled (ZFC) magnetic susceptibility in $Fe_{1+y}Te_{1-x}Se_x$ samples 1 to 6. The resistivity in sample 6 is multiplied by 10 for clarity and plotted in (a).

superconductivities for different sectional crystals in the grown ingot in which the actual composition and extra iron in the crystals are variable. Sample 5 is the as-grown sample and has the lowest superconductivity temperature. As-grown $Fe_{1+y}Te_{1-x}Se_x$ single crystals were sealed in a vacuum quartz tube and annealed with different conditions. Samples 1 and 2 are annealed at 400 °C for 50 days. Sample 3 is annealed at 450 °C for 6 days, sample 4 is annealed at 400 °C for 7 days. Sample 6 is single crystal without excess Fe, usually without shinning surface and superconducting without postannealing.

Resistivity and magnetization were measured in a Physical Properties Measurement System (PPMS) DynaCool from Quantum Design and shown in Fig. 5. $Fe_{1+y}Te_{1-x}Se_x$ sample 1 has the highest T_c and second lowest resistivity while sample 5 has the lowest T_c and highest resistivity. Sample 6 has the lowest resistivity. The zero-field-cooled (ZFC) magnetization was measured with the magnetic field applied inside the *ab* plane of the crystal. The superconducting transition temperature T_c was defined as the temperature where resistivity drops to one-half. The superconductivity fractional volume (SFV) was calculated from the ZFC data. Refer to Table I for more details.

2. Supplementary text

a. Data analysis

When we analyze the data, the intrinsic Nernst signal N_S is obained by subtracting the thermopower signal, viz.,

$$N_S(B,T) = e_N(B,T) - kS(B,T) \qquad \text{(A1)}$$

in which k is a geometrical scaling factor. The geometrical scaling factor should be the same when the temperature is above or below the superconducting transition temperature. Indeed, whether the thermopower is isotropic or could not be decided by heat-current direction. With a well-defined sample geometry, the heat should transfer uniformly inside the sample. At such a low-temperature range ($T < 20$ K), the heat transport is mainly conducted by phonons, which means crystal structure decides the heat-flow anisotropy in the sample. For the samples studied in this work, the Se doping level x is between 0.3 and 0.45. In such a doping region, the crystal structure does not change down to the lowest temperature. In all, we believe that the direction of heat flow remains unchanged as the sample enters the superconducting state.

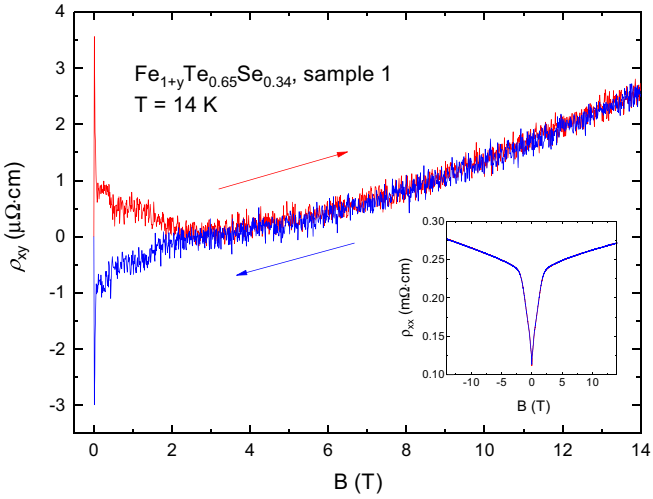

FIG. 6. The Hall resistivity ρ_{xy} measured at 14 K in $Fe_{1+y}Te_{0.65}Se_{0.34}$ sample 1. The inset shows the magnetoresistivity ρ_{xx} measured at the same temperature. Red curve represents the field sweep up while blue curve represents the sweep down.

b. Hall signal in $Fe_{1+y}Te_{0.65}Se_{0.34}$ *sample 1*

We measured the Hall signal in $Fe_{1+y}Te_{0.65}Se_{0.34}$ sample 1 up to 14 T at the temperature where the spontaneous Nernst signal is the largest. Figure 6 shows the Hall resistivity ρ_{xy} measured during field sweep up and sweep down. The inset of Fig. 6 shows the magnetoresistivity ρ_{xx} measured at the same temperature. At 14 T, $\frac{\rho_{xy}}{\rho_{xx}} < 0.01$, which means the Hall angle $\theta < 0.57^\circ$ and can be neglected when we calculate the Peltier Hall angle θ^P. With the Nernst signal e_y and Seebeck coefficient, we can get

$$e_N = S(\alpha_{xy}/\alpha - \sigma_{xy}/\sigma) = S(\tan\theta^P - \tan\theta) \approx S\tan\theta^P, \tag{A2}$$

$$\tan\theta^P \approx e_y/S \tag{A3}$$

in which σ_{xy} is the Hall conductivity, e_N is the Nernst signal, and α is the 2D Peltier conductivity tensor.

c. Spontaneous Nernst signal with different cooling process

The local magnetic moments introduced by impurity ions are pinned randomly in the sample, which means the Ising-type magnetic moment could either point up or down in the zero-field-cooling process. We tried to change the magnetic moment direction of interstitial Fe by warming up the sample to 350 K and do a field cooling in both $B = 14$ and -14 T, then swept the field between 14 and -14 T at several temperatures where the unusual Nernst signal is most prominent [as shown in Fig. 7(d)]. We also did a T sweep below 20 K to check the zero-field Nernst signal [as shown in Figs. 7(b) and 7(c)]. The results show that the field-cooling process can not alter the sign or the magnitude of the spontaneous Nernst signal. One possibility is 350 K is not high enough to overcome the large out-of-plane magnetic anisotropy energy or alter the magnetic moment direction.

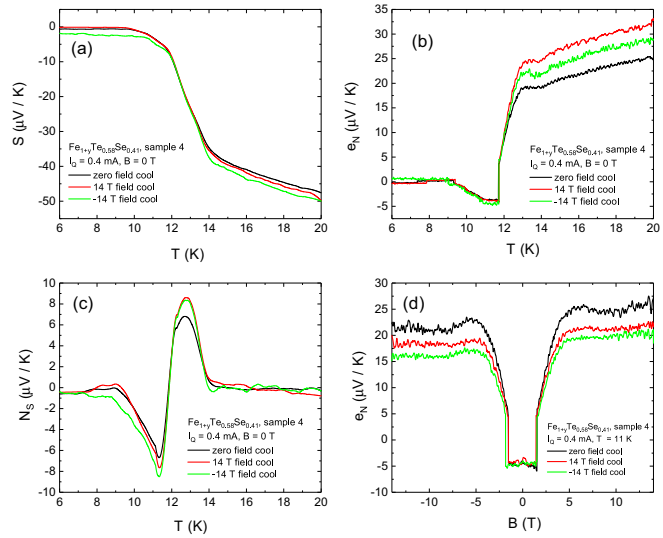

FIG. 7. The Seebeck and Nernst signals measured with different cooling process in $Fe_{1+y}Te_{1-x}Se_x$ sample 4. Temperature T dependence of the (a) thermopower S (Seebeck signal) and (b) the observed Nernst signal e_N in sample 4. (c) The intrinsic spontaneous Nernst signal is extracted by subtracting the scaled thermopower signal $N_S(T) = e_N(T) - kS(T)$. (d) Observed Nernst signal e_N vs magnetic field B at 11 K in sample 4. Black curves are taken with zero-field-cooled process. Red curves are taken with a 14-T field-cooled process. Green curves are taken with a -14-T field-cooled process. The field was applied at 350 K.

d. Complete data set for $Fe_{1+y}Te_{1-x}Se_x$ *samples 2 to 6*

Figure 8 shows the zero-field Seebeck signal S and Nernst signal e_N measured in all $Fe_{1+y}Te_{1-x}Se_x$ samples. For samples 1, 2, and 4, two Nernst channels are measured. For samples 3, 5, and 6, three Nernst channels are measured. Take sample 3 as an example [as shown in Fig. 8(c)], the magnitude and sign of the spontaneous Nernst signal across T_c (~14 K) are different among three Nernst channels. The spontaneous Nernst signal on channels e_{N1} and e_{N2} are negative while e_{N3} is positive. The field-dependent data for $Fe_{1+y}Te_{1-x}Se_x$ sample 1 has been presented in the main text. Figures 9–13 plot the field-dependent data for $Fe_{1+y}Te_{1-x}Se_x$ samples 2 to 6.

e. Complete data set for FeSe

Figure 14 plots the complete data set for FeSe sample 1. The FeSe single crystal being measured here has a dimension of $2.5 \times 1 \times 0.175$ mm^3 and a superconducting transition temperature of $T_c \sim 8.3$ K. Figure 14(a) shows two Nernst channels only have pickup from the Seebeck signal. There is no obvious zero-field Nernst signal across the superconducting transition. Figure 14(b) plots the field-dependent Nernst signal e_{N3}, which is dominated by the antisymmetric ordinary Nernst signal. The ordinary Nernst signal N_{AS} of FeSe sample 1 following the standard B antisymmetrization to curves in Fig. 14(b) is shown in Fig. 14(d), which is about two times the value obtained in Ref. [59].

f. Thermal Hall measurement in $Fe_{1+y}Te_{1-x}Se_x$ *sample 1*

Our analysis assumes that the temperature gradient in our sample is homogeneous. A horizontal thermal gradient

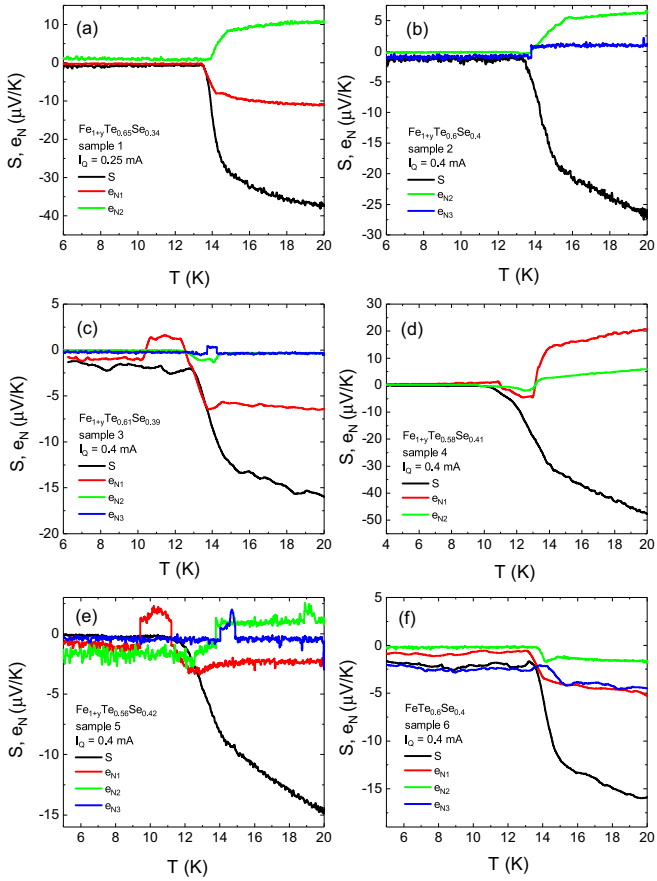

FIG. 8. The zero-field Seebeck signal S and Nernst signal e_N measured in $Fe_{1+y}Te_{1-x}Se_x$ samples 1 to 6. For samples 1, 2, and 4, two Nernst channels are measured. For samples 3, 5, and 6, three Nernst channels are measured. The heater resistance is 1 kΩ for all the samples.

component may induce a horizontal voltage that looks as a Nernst effect signal. To check if this horizontal thermal gradient exists, we carried out the thermal Hall measurement in $Fe_{1+y}Te_{1-x}Se_x$ sample 1 at $B = 1$ and 4 T. The data are shown in Fig. 15. At both 1 and 4 T, the thermal Hall signal is around zero with a finite noise level. Our experiment shows that no thermal Hall signal has been observed at either zero field or finite field. So, we believe there is no large transverse thermal gradient component built up in the samples at zero magnetic field, which indicates a homogeneous thermal gradient across the sample. We note that a spontaneous thermal Hall effect is highly unusual and has only been reported in very few materials, such as the chiral antiferromagnet Mn_3Sn [64].

g. Discussion about sample disorder, inhomogeneity, contact misalignment, and anisotropic Seebeck pickup

The inhomogeneity and nanoscale electronic disorder in the high-T_c superconductors have been observed in many cuprates [61–63]. This electronic inhomogeneity is commonly attributed to a disorder introduced by the poorly screened electrostatic potential of the out-of-plane oxygen dopant atoms [65,66], although the electronic inhomogeneity is also argued to be intrinsic to the competing orders. But, this electronic inhomogeneity does not generally induce a spontaneous

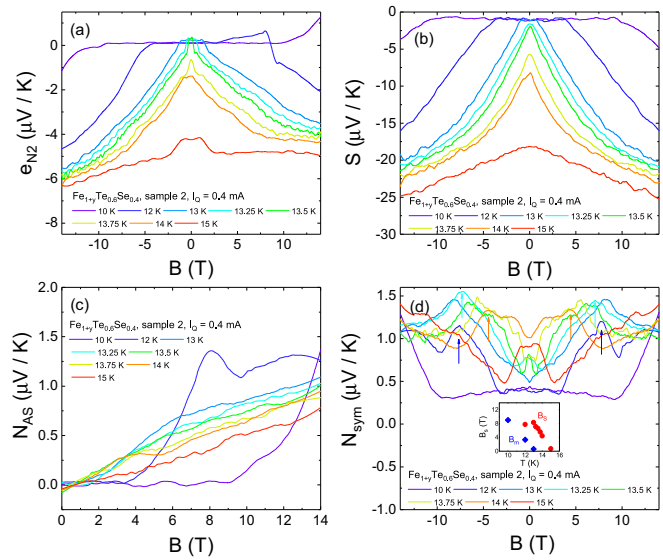

FIG. 9. Observed (a) Nernst signal e_{N2} and (b) Seebeck signal vs magnetic field B at selected T from 10 to 15 K in sample 2. (c) Ordinary Nernst signal N_{AS} of sample 2 following the standard B antisymmetrization to curves in (a). (d) Magnetic field dependence of the intrinsic field-symmetrized Nernst signal. Arrows indicate the location of the shoulder trend B_S. The Seebeck pickup has been subtracted. Inset shows the temperature dependence of B_S, compared with the melting fields B_m. As expected for the characteristic field scales in superconductors, both fields converge to zero as the T increases toward T_c. The heater resistance is 1 kΩ.

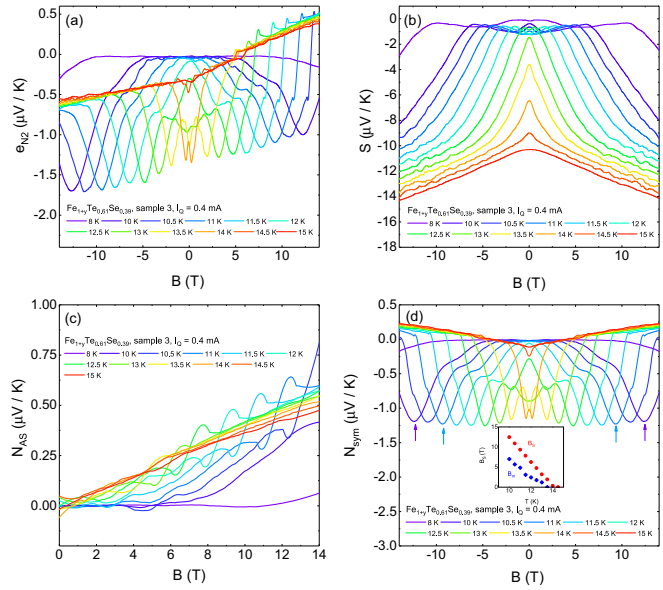

FIG. 10. Observed (a) Nernst signal e_{N2} and (b) Seebeck signal vs magnetic field B at selected T from 8 to 15 K in sample 3. (c) Ordinary Nernst signal N_{AS} of sample 3 following the standard B antisymmetrization to curves in (a). (d) Magnetic field dependence of the intrinsic field-symmetrized Nernst signal. Arrows indicate the location of the shoulder trend B_S. The Seebeck pickup has been subtracted. Inset shows the temperature dependence of B_S, compared with the melting fields B_m. As expected for the characteristic field scales in superconductors, both fields converge to zero as the T increases toward T_c. The heater resistance is 1 kΩ.

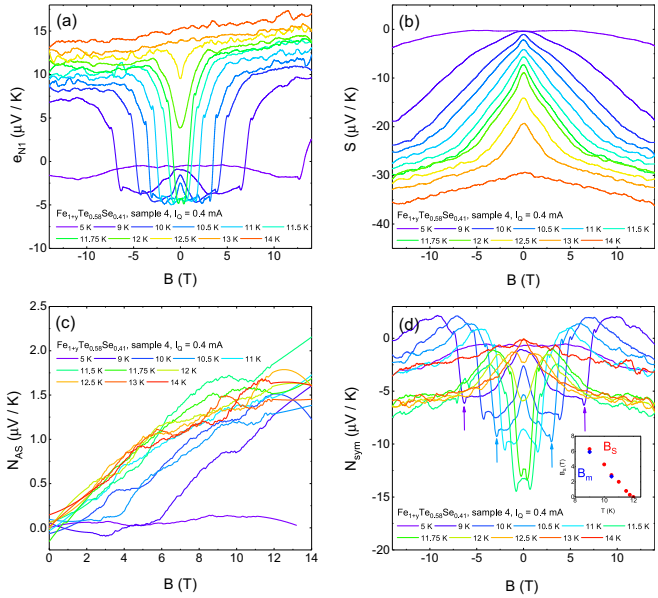

FIG. 11. Observed (a) Nernst signal e_{N1} and (b) Seebeck signal vs magnetic field B at selected T from 5 to 14 K in sample 4. (c) Ordinary Nernst signal N_{AS} of sample 4 following the standard B antisymmetrization to curves in (a). (d) Magnetic field dependence of the intrinsic field-symmetrized Nernst signal. Arrows indicate the location of the shoulder trend B_S. The Seebeck pickup has been subtracted. Inset shows the temperature dependence of B_S, compared with the melting fields B_m. As expected for the characteristic field scales in superconductors, both fields converge to zero as the T increases toward T_c. The heater resistance is 1 kΩ.

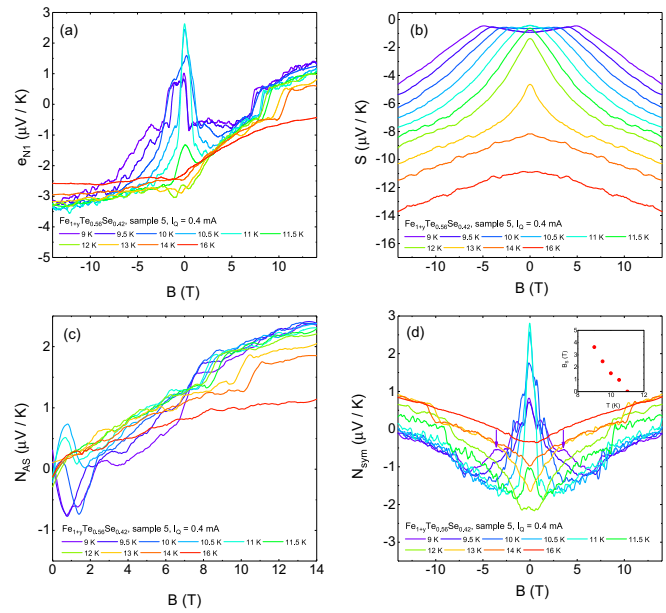

FIG. 12. Observed (a) Nernst signal e_{N1} and (b) Seebeck signal vs magnetic field B at selected T from 9 to 16 K in sample 5. (c) Ordinary Nernst signal N_{AS} of sample 5 following the standard B antisymmetrization to curves in (a). (d) Magnetic field dependence of the intrinsic field-symmetrized Nernst signal. Arrows indicate the location of the shoulder trend B_S. The Seebeck pickup has been subtracted. Inset shows the temperature dependence of B_S, compared with the melting fields B_m. As expected for the characteristic field scales in superconductors, both fields converge to zero as the T increases toward T_c. The heater resistance is 1 kΩ.

Nernst signal in the vortex liquid states of these cuprates, with the only exception of the $\frac{1}{8}$-doped striped-phased LBCO [20]. Obviously, the spontaneous Nernst signal does not result simply from the inhomogeneity in a vortex liquid. It must be related to some intrinsic properties of the material $Fe_{1+y}Te_{1-x}Se_x$.

The spontaneous Nernst signal does not come from the misalignment of the Nernst channel contacts either because our $Fe_{1+y}Te_{1-x}Se_x$ and FeSe samples have similar contact misalignment conditions and FeSe sample does not show a large spontaneous Nernst signal under fields. Furthermore, the spontaneous Nernst signal does not come from the pickup of anisotropic thermopower signal. At such a low-temperature range ($T < 20$ K), the heat transport is mainly conducted by phonons, which means crystal structure decides the heat-flow anisotropy in the sample. $Fe_{1+y}Te_{1-x}Se_x$ sample has a tetragonal structure while FeSe has an orthogonal structure at this temperature range. When we apply the heat current in plane, the FeSe sample could have a more anisotropic thermopower signal. But, we do not observe the zero-field Nernst signal in FeSe even with the same data analysis method, which indicates this zero-field Nernst signal may not purely come from an anisotropic Seebeck pickup.

In order to further verify that the spontaneous Nernst signal is not simply coming from the pickup of inhomogeneous Seebeck signals, we measure three pairs of Seebeck channels in $Fe_{1+y}Te_{1-x}Se_x$ sample 1. The experimental configuration is shown in Fig. 16(a). The Seebeck channels measured here are

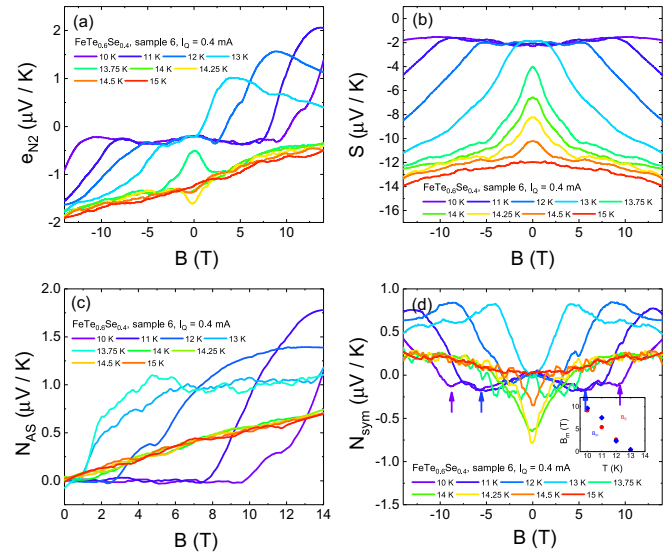

FIG. 13. Observed (a) Nernst signal e_{N2} and (b) Seebeck signal vs magnetic field B at selected T from 10 to 15 K in sample 6. (c) Ordinary Nernst signal N_{AS} of sample 6 following the standard B antisymmetrization to curves in (a). (d) Magnetic field dependence of the intrinsic field-symmetrized Nernst signal. Arrows indicate the location of the shoulder trend B_S. The Seebeck pickup has been subtracted. Inset shows the temperature dependence of B_S, compared with the melting fields B_m. As expected for the characteristic field scales in superconductors, both fields converge to zero as the T increases toward T_c. The heater resistance is 1 kΩ.

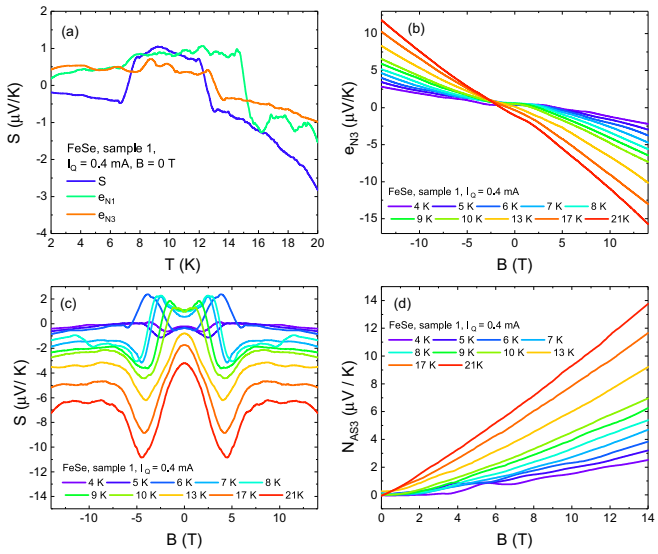

FIG. 14. (a) Observed Nernst signal e_{N1}, e_{N3} and Seebeck signal S vs T at $B = 0$ T for FeSe sample 1. Observed (b) Nernst signal e_{N3} and (c) Seebeck signal S vs magnetic field B at selected T from 4 to 21 K in FeSe sample 1. (d) Ordinary Nernst signal N_{AS} of FeSe sample 1 following the standard B antisymmetrization to curves in (b). The heater resistance is 1 kΩ.

S_1 and S_1', S_2 and S_2', S_3 and S_3'. Each pair of them are measured simultaneously. In order to align the contacts of corresponding Seebeck channels well, the contacts are remade with silver epoxy. The distance between contacts V_{1A} and V_{2A} is 0.9 mm, which is the same as the distance between contacts V_{1A}' and V_{2A}'. The distance between contacts V_{2A} and V_{3A} is 0.875 mm, which is a little bit shorter than the distance between contacts V_{2A}' and V_{3A}' (0.9 mm).

Figures 16(b)–16(d) show the experimental results. Figure 16(b) is the measured Seebeck coefficient S vs T of channels S_1 and S_1'. S_1' vs T overlaps with S_1 vs T after

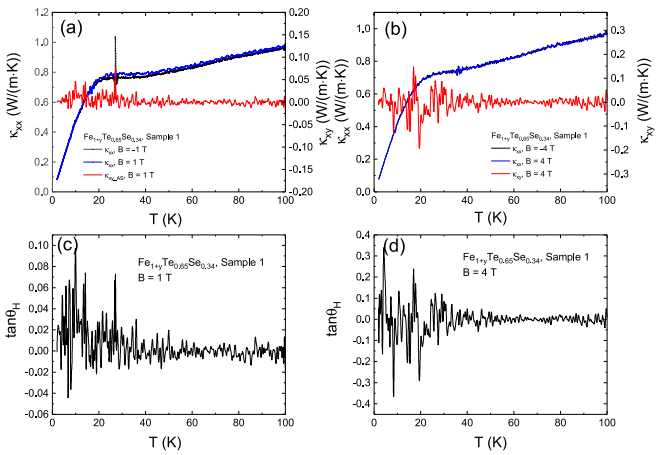

FIG. 15. Thermal conductivity κ_{xx} and thermal Hall conductivity κ_{xy} measured in $Fe_{1+y}Te_{0.65}Se_{0.34}$ sample 1 at (a) $B = 1$ T and (b) $B = 4$ T. The thermal Hall angle θ_H is extracted from the ratio of the thermal Hall conductivity and thermal conductivity with $\tan\theta_H = \frac{\kappa_{xy}}{\kappa_{xx}}$.

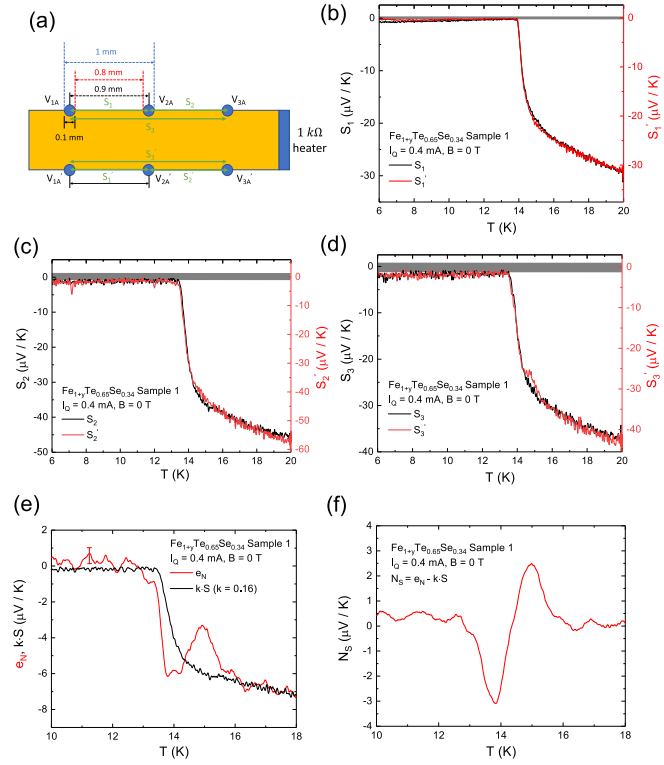

FIG. 16. (a) Experimental configuration of $Fe_{1+y}Te_{1-x}Se_x$ sample 1, which is the same as the $Fe_{1+y}Te_{1-x}Se_x$ sample 1 configuration in the main text. Six contacts were remade to make sure they are well aligned. S_x and $S_{x'}$ are two Seebeck channels being measured simultaneously. Blue solid circles are electrical contacts. Dashed lines and arrows label the distance between the contacts. (b)–(d) Measured Seebeck coefficients for three pairs of Seebeck channels. The Seebeck coefficients of channel S_1' overlap with channel S_1 after multiplying by a factor of 0.94. The scaling factor between Seebeck channels S_2 and S_2', S_3 and S_3' are 0.84 and 0.87. Gray solid lines mark $S = 0$ with their widths indicate the error bar of the Seebeck coefficient. The heater resistance is 1 kΩ. The heater current is 0.4 mA. (e) Temperature dependence of the thermopower kS (Seebeck signal) and the observed Nernst signal e_N in sample 1. The thermopower signal S was scaled by a factor $k = 0.16$ to match the T dependence of S and e_N. (f) The intrinsic spontaneous Nernst signals N_S vs T in sample 1, which is extracted by subtracting the scaled thermopower signal $N_S(T) = e_N(T) - kS(T)$.

multiplying by a factor of 0.94. The scaling factor between Seebeck channels S_2 and S_2', S_3 and S_3' are 0.84 and 0.87. The difference between S_x and S_x' is within the error bar brought by the size of the electrical contacts and the slight misalignment of the contacts. Take S_1 and S_1' as an example, the electrical contacts are made by silver epoxy and have a diameter of 0.1 mm. Compared to the distance between the two contacts, which is 0.9 mm, it can bring an error of -10% to $+12.5\%$ to the Seebeck coefficient.

If we define T_c to be the temperature where the Seebeck signal changes from nearly zero to a finite value, we can see that Seebeck channels S_x and S_x' resolve exactly the same T_c. Therefore, two edges of our sample do not have large inhomogeneity, which can bring different T_c for Seebeck channels S_x and S_x'. But, the T_c for S_1, S_2, and S_3 are 13.9, 13.4,

and 13.5 K, which are different. This is due to the temperature gradient that built up along the sample. The actual temperature differs for about 0.5 K between the hot and cold ends of the sample.

Furthermore, the difference between Seebeck channels S_x and S'_x has a monotonic dependence with temperature which increases from a near-zero value to a finite value when it enters the normal state. In contrast, the zero-field Nernst signal shows a nonmonotonic dependence with temperature [such as Fig. 1(c) in the main text of our paper], which can not come from the contribution of a monotonic Seebeck pickup.

Besides, we also measured the Nernst signal in $Fe_{1+y}Te_{1-x}Se_x$ sample 1 after remaking the contacts. Sample 1 still shows a spontaneous Nernst signal at $B = 0$ T [as shown in Figs. 16(e) and 16(f)]. The magnitude of the spontaneous Nernst signal e_N is comparable to the result in Fig. 1(c) in the main text of our paper, which is taken before remaking the contacts. We note that the temperature dependence of the e_N is different from what is measured with the original contacts. We suspect that is due to the inhomogeneity of the Fe impurities in the sample. Similar patterns are observed in other samples, like those in Fig. 7(c).

In conclusion, the measured Seebeck coefficients verify the homogeneity of our sample. As a result, the zero-field Nernst signal is not simply due to the pickup of inhomogeneous Seebeck signal and is intrinsic to the $Fe_{1+y}Te_{1-x}Se_x$ samples.

[1] C. Nayak, S. H. Simon, A. Stern, M. Freedman, and S. Das Sarma, Rev. Mod. Phys. **80**, 1083 (2008).

[2] X.-L. Qi and S.-C. Zhang, Rev. Mod. Phys. **83**, 1057 (2011).

[3] Z. Wang, P. Zhang, G. Xu, L. K. Zeng, H. Miao, X. Xu, T. Qian, H. Weng, P. Richard, A. V. Fedorov, H. Ding, X. Dai, and Z. Fang, Phys. Rev. B **92**, 115119 (2015).

[4] X. Wu, S. Qin, Y. Liang, H. Fan, and J. Hu, Phys. Rev. B **93**, 115129 (2016).

[5] G. Xu, B. Lian, P. Tang, X.-L. Qi, and S.-C. Zhang, Phys. Rev. Lett. **117**, 047001 (2016).

[6] P. Zhang, K. Yaji, T. Hashimoto, Y. Ota, T. Kondo, K. Okazaki, Z. Wang, J. Wen, G. D. Gu, H. Ding, and S. Shin, Science **360**, 182 (2018).

[7] D. Wang, L. Kong, P. Fan, H. Chen, S. Zhu, W. Liu, L. Cao, Y. Sun, S. Du, J. Schneeloch, R. Zhong, G. Gu, L. Fu, H. Ding, and H.-J. Gao, Science **362**, 333 (2018).

[8] L. Kong, S. Zhu, M. Papaj, H. Chen, L. Cao, H. Isobe, Y. Xing, W. Liu, D. Wang, P. Fan, Y. Sun, S. Du, J. Schneeloch, R. Zhong, G. Gu, L. Fu, H.-J. Gao, and H. Ding, Nat. Phys. **15**, 1181 (2019).

[9] X. Chen, M. Chen, W. Duan, X. Zhu, H. Yang, and H.-H. Wen, arXiv:1909.01686.

[10] J.-X. Yin, Z. Wu, J.-H. Wang, Z.-Y. Ye, J. Gong, X.-Y. Hou, L. Shan, A. Li, X.-J. Liang, X.-X. Wu, J. Li, C.-S. Ting, Z.-Q. Wang, J.-P. Hu, P.-H. Hor, H. Ding, and S. H. Pan, Nat. Phys. **11**, 543 (2015).

[11] K. Jiang, X. Dai, and Z. Wang, Phys. Rev. X **9**, 011033 (2019).

[12] J. Wen, G. Xu, G. Gu, J. M. Tranquada, and R. J. Birgeneau, Rep. Prog. Phys. **74**, 124503 (2011).

[13] L. Chen, Z. Xiang, C. Tinsman, T. Asaba, Q. Huang, H. Zhou, and L. Li, Appl. Phys. Lett. **113**, 061902 (2018).

[14] L. Chen, Z. Xiang, C. Tinsman, Q. Huang, K. G. Reynolds, H. Zhou, and L. Li, Appl. Phys. Lett. **114**, 251904 (2019).

[15] Y. Wang, L. Li, and N. P. Ong, Phys. Rev. B **73**, 024510 (2006).

[16] L. Li, Y. Wang, M. J. Naughton, S. Komiya, S. Ono, Y. Ando, and N. P. Ong, J. Magn. Magn. Mater. **310**, 460 (2007).

[17] Y. Onose, L. Li, C. Petrovic, and N. P. Ong, Europhys. Lett. **79**, 17006 (2007).

[18] J. Chang, R. Daou, C. Proust, D. LeBoeuf, N. Doiron-Leyraud, F. Laliberté, B. Pingault, B. J. Ramshaw, R. Liang, D. A. Bonn, W. N. Hardy, H. Takagi, A. B. Antunes, I. Sheikin, K. Behnia, and L. Taillefer, Phys. Rev. Lett. **104**, 057005 (2010).

[19] K. Behnia, J. Phys.: Condens. Matter **21**, 113101 (2009).

[20] L. Li, N. Alidoust, J. M. Tranquada, G. D. Gu, and N. P. Ong, Phys. Rev. Lett. **107**, 277001 (2011).

[21] A. Pourret, Liam Malone, A. B. Antunes, C. S. Yadav, P. L. Paulose, B. Fauqué, and K. Behnia, Phys. Rev. B **83**, 020504(R) (2011).

[22] H.-C. Ri, R. Gross, F. Gollnik, A. Beck, R. P. Huebener, P. Wagner, and H. Adrian, Phys. Rev. B **50**, 3312 (1994).

[23] Y. Wang, N. P. Ong, Z. A. Xu, T. Kakeshita, S. Uchida, D. A. Bonn, R. Liang, and W. N. Hardy, Phys. Rev. Lett. **88**, 257003 (2002).

[24] M.-S. Nam, A. Ardavan, S. J. Blundell, and J. A. Schlueter, Nature (London) **449**, 584 (2007).

[25] A. Pourret, P. Spathis, H. Aubin, and K. Behnia, New J. Phys. **11**, 055071 (2009).

[26] C. M. Varma, Phys. Rev. B **55**, 14554 (1997).

[27] C. M. Varma, Phys. Rev. Lett. **83**, 3538 (1999).

[28] W.-C. Lee, S.-C. Zhang, and C. Wu, Phys. Rev. Lett. **102**, 217002 (2009).

[29] S. Maiti and A. V. Chubukov, Phys. Rev. B **87**, 144511 (2013).

[30] M. Marciani, L. Fanfarillo, C. Castellani, and L. Benfatto, Phys. Rev. B **88**, 214508 (2013).

[31] J. Kang, A. V. Chubukov, and R. M. Fernandes, Phys. Rev. B **98**, 064508 (2018).

[32] A. Kaminski, S. Rosenkranz, H. M. Fretwell, J. C. Campuzano, Z. Li, H. Raffy, W. G. Cullen, H. You, C. G. Olsonk, C. M. Varma, and H. Höchst, Nature (London) **416**, 610 (2002).

[33] B. Fauqué, Y. Sidis, V. Hinkov, S. Pailhes, C. T. Lin, X. Chaud, and P. Bourges, Phys. Rev. Lett. **96**, 197001 (2006).

[34] H. A. Mook, Y. Sidis, B. Fauqué, V. Balédent, and P. Bourges, Phys. Rev. B **78**, 020506(R) (2008).

[35] Y. Li, V. Balédent, N. Barišić, Y. Cho, B. Fauqué, Y. Sidis, G. Yu, X. Zhao, P. Bourges, and M. Greven, Nature (London) **455**, 372 (2008).

[36] A. Soumyanarayanan, X. Y. Tee, T. Ito, T. Ushiyama, Y. Tomioka, and C. Panagopoulos, Phys. Rev. B **93**, 054512 (2016).

[37] J. Xia, Elizabeth Schemm, G. Deutscher, S. A. Kivelson, D. A. Bonn, W. N. Hardy, R. Liang, W. Siemons, G. Koster, M. M. Fejer, and A. Kapitulnik, Phys. Rev. Lett. **100**, 127002 (2008).

[38] R.-H. He, M. Hashimoto, H. Karapetyan, J. D. Koralek, J. P. Hinton, J. P. Testaud, V. Nathan, Y. Yoshida, H. Yao, K. Tanaka,

W. Meevasana, R. G. Moore, D. H. Lu, S.-K. Mo, M. Ishikado, H. Eisaki, Z. Hussain, T. P. Devereaux, S. A. Kivelson *et al.*, Science **331**, 1579 (2011).

[39] H. Karapetyan, M. Hücker, G. D. Gu, J. M. Tranquada, M. M. Fejer, Jing Xia, and A. Kapitulnik, Phys. Rev. Lett. **109**, 147001 (2012).

[40] V. Grinenko, P. Materne, R. Sarkar, H. Luetkens, K. Kihou, C. H. Lee, S. Akhmadaliev, D. V. Efremov, S.-L. Drechsler, and H.-H. Klauss, Phys. Rev. B **95**, 214511 (2017).

[41] S. Li, C. de la Cruz, Q. Huang, Y. Chen, J. W. Lynn, J. Hu, Y.-L. Huang, F.-C. Hsu, K.-W. Yeh, M.-K. Wu, and P. Dai, Phys. Rev. B **79**, 054503 (2009).

[42] W. Bao, Y. Qiu, Q. Huang, M. A. Green, P. Zajdel, M. R. Fitzsimmons, M. Zhernenkov, S. Chang, Minghu Fang, B. Qian, E. K. Vehstedt, Jinhu Yang, H. M. Pham, L. Spinu, and Z. Q. Mao, Phys. Rev. Lett. **102**, 247001 (2009).

[43] J. D. Rameau, N. Zaki, G. D. Gu, P. D. Johnson, and M. Weinert, Phys. Rev. B **99**, 205117 (2019).

[44] Z. A. Xu, N. P. Ong, Y. Wang, T. Kakeshita, and S. Uchida, Nature (London) **406**, 486 (2000).

[45] O. Cyr-Choinière, R. Daou, F. Laliberté, D. LeBoeuf, N. Doiron-Leyraud, J. Chang, J.-Q. Yan, J.-G. Cheng, J.-S. Zhou, J. B. Goodenough, S. Pyon, T. Takayama, H. Takagi, Y. Tanaka, and L. Taillefer, Nature (London) **458**, 743 (2009).

[46] F. F. Tafti, F. Laliberté, M. Dion, J. Gaudet, P. Fournier, and L. Taillefer, Phys. Rev. B **90**, 024519 (2014).

[47] J. Chang, N. Doiron-Leyraud, O. Cyr-Choinière, G. Grissonnanche, F. Laliberté, E. Hassinger, J.-Ph. Reid, R. Daou, S. Pyon, T. Takayama, H. Takagi, and L. Taillefer, Nat. Phys. **8**, 751 (2012).

[48] Y. Wang, Nernst effect in high temperature superconductors, Ph.D. thesis, Princeton University, 2004.

[49] E. Berg, E. Fradkin, S. A. Kivelson, and J. M. Tranquada, New J. Phys. **11**, 115004 (2009).

[50] Q. Li, M. Hücker, G. D. Gu, A. M. Tsvelik, and J. M. Tranquada, Phys. Rev. Lett. **99**, 067001 (2007).

[51] J. M. Tranquada, G. D. Gu, M. Hücker, Q. Jie, H.-J. Kang, R. Klingeler, Q. Li, N. Tristan, J. S. Wen, G. Y. Xu, Z. J. Xu, J. Zhou, and M. v. Zimmermann, Phys. Rev. B **78**, 174529 (2008).

[52] A. Kondrat, G. Behr, B. Büchner, and C. Hess, Phys. Rev. B **83**, 092507 (2011).

[53] K. Behnia and H. Aubin, Rep. Prog. Phys. **79**, 046502 (2016).

[54] A. A. Kalenyuk, A. Pagliero, E. A. Borodianskyi, S. Aswartham, S. Wurmehl, B. Büchner, D. A. Chareev, A. A. Kordyuk, and V. M. Krasnov, Phys. Rev. B **96**, 134512 (2017).

[55] D. S. Fisher, M. P. A. Fisher, and D. A. Huse, Phys. Rev. B **43**, 130 (1991).

[56] L. N. Bulaevskii, M. Ledvij, and V. G. Kogan, Phys. Rev. Lett. **68**, 3773 (1992).

[57] Y. Sun, Y. Tsuchiya, T. Taen, T. Yamada, S. Pyon, A. Sugimoto, T. Ekino, Z. Shi, and T. Tamegai, Sci. Rep. **4**, 4585 (2014).

[58] K. Nakayama, Y. Miyata, G. N. Phan, T. Sato, Y. Tanabe, T. Urata, K. Tanigaki, and T. Takahashi, Phys. Rev. Lett. **113**, 237001 (2014).

[59] H. Yang, G. Chen, X. Zhu, J. Xing, and H.-H. Wen, Phys. Rev. B **96**, 064501 (2017).

[60] R. Hu, H. Lei, M. Abeykoon, E. S. Bozin, S. J. L. Billinge, J. B. Warren, T. Siegrist, and C. Petrovic, Phys. Rev. B **83**, 224502 (2011).

[61] K. McElroy, J. Lee, J. A. Slezak, D.-H. Lee, H. Eisaki, S. Uchida, and J. C. Davis, Science **309**, 1048 (2005).

[62] H. Mashima, N. Fukuo, Y. Matsumoto, G. Kinoda, T. Kondo, H. Ikuta, T. Hitosugi, and T. Hasegawa, Phys. Rev. B **73**, 060502(R) (2006).

[63] D. Pelc, M. Vučković, M. S. Grbić, M. Požek, G. Yu, T. Sasagawa, M. Greven, and N. Barišić, Nat. Commun. **9**, 4327 (2018).

[64] X. Li, L. Xu, L. Ding, J. Wang, M. Shen, X. Lu, Z. Zhu, and K. Behnia, Phys. Rev. Lett. **119**, 056601 (2017).

[65] Z. Wang, J. R. Engelbrecht, S. Wang, H. Ding, and S. H. Pan, Phys. Rev. B **65**, 064509 (2002).

[66] A. V. Balatsky, I. Vekhter, and J.-X. Zhu, Rev. Mod. Phys. **78**, 373 (2006).